

A nucleolar protein, *H19* opposite tumor suppressor (*HOTS*), is a tumor growth inhibitor encoded by a human imprinted *H19* antisense transcript

Patrick Onyango and Andrew P. Feinberg¹

Center for Epigenetics and Department of Medicine, The Johns Hopkins University School of Medicine, Baltimore, MD 21205

Edited by Bert Vogelstein, The Johns Hopkins University, Baltimore, MD, and approved September 1, 2011 (received for review July 6, 2011)

The *H19* gene, which localizes within a chromosomal region on human chromosome 11p15 that is commonly lost in Wilms tumor (WT), encodes an imprinted untranslated RNA. However, the biological significance of the *H19* noncoding transcript remains unresolved because replacement of the RNA transcript with a neocassette has no obvious phenotypic effect. Here we show that the human *H19* locus also encodes a maternally expressed, translated gene, antisense to the known *H19* transcript, which is conserved in primates. This gene, termed *HOTS* for *H19* opposite tumor suppressor, encodes a protein that localizes to the nucleus and nucleolus and that interacts with the human enhancer of rudimentary homolog (ERH) protein. WTs that show loss of heterozygosity of 11p15 or loss of imprinting of *IGF2* also silence *HOTS* (7/7 and 10/10, respectively). Overexpression of *HOTS* inhibits Wilms, rhabdoid, rhabdomyosarcoma, and choriocarcinoma tumor cell growth, and silencing *HOTS* by RNAi increases *in vitro* colony formation and *in vivo* tumor growth. These results demonstrate that the human *H19* locus harbors an imprinted gene encoding a tumor suppressor protein within the long-sought WT2 locus.

antisense RNA | DNA methylation | epigenetics | genomic | imprinting

Genomic imprinting is an epigenetic modification leading to parent-of-origin-dependent differential expression of the two alleles of a gene. Much of our knowledge of this phenomenon comes from studies of the maternally expressed *H19* and the nearby imprinted *Igf2* gene, which is reciprocally expressed from the paternal allele (1). In the past decade, several deletion mutants and transgenic mouse models targeting the *H19-Igf2* locus have been developed (1). These studies show that regulation of *Igf2* and *H19* imprinting is dependent on a differentially methylated region (DMR) located -4 to -2 kb upstream from the *H19* transcriptional start site (2–4). Only when the DMR is unmethylated does the methylation-sensitive zinc-finger protein CTCF bind, thus insulating *Igf2* from its enhancer creating a silenced maternal *Igf2* allele (5, 6). Knockout of the mouse *H19* transcript has provided mixed results; in one case, no function was inferred (7), and in another case, overgrowth was reported due to activation of the normally silent paternal allele of *Igf2*, an important autocrine growth factor (4, 8). In humans, loss of imprinting (LOI) of *IGF2* is an important epigenetic mechanism first found in WT (9), the most common childhood kidney cancer; in Beckwith–Wiedemann syndrome (BWS) (10), which predisposes to WT; and in many other childhood and adult malignancies (11). LOI can also be caused, at least in BWS, by microdeletions within the *H19* DMR (12), although most loss of heterozygosity (LOH) in WT includes *IGF2* itself (13) and so presumably acts through a mechanism other than LOI. In addition to LOI of *IGF2*, about 30% of WTs and other embryonal tumors show LOH of 11p15, which has been narrowed down to a 1-Mb region including the *H19* gene (13–15). LOH of 11p15 is also commonly found in rhabdomyosarcoma, rhabdoid, cervical, ovarian, lung, bladder, breast, and hepatocellular cancers (13, 15). Preferential LOH of the maternal allele in WT and embryonal tumors implies that the undiscovered WT2 gene is

imprinted and expressed from the maternal allele (16). However, no imprinted tumor suppressor gene in this region has yet been identified. The maternally expressed imprinted gene *CDKN1C* is not a likely candidate gene because it is expressed even in LOH-positive WT (17). There are also contradictory data on the role of *H19* in cancer, as the sense RNA has been described by some as an oncogene (18) and others have demonstrated that the transfected *H19* gene suppresses cellular proliferation, clonogenicity, and tumorigenicity in certain tumor cell lines (19). Moreover, recent studies on the *H19* locus have identified the *H19*-derived miR-675 and a *H19* antisense RNA named *91H* (20, 21). The miR-675 targets and down-regulates the *RB* gene and is thought to contribute to colorectal cancer development when overexpressed (20), and *91H* is a single 120-kb transcript that is stabilized in breast cancer cells and overexpressed in human breast tumors (21). Because the *H19* loci is inactive in WT due to LOH or imprinting, neither of these recent studies demonstrate a tumor suppressor role for the *H19* locus. Other large intervening noncoding RNAs (lincRNAs) like *HOTAIR* show increased expression in primary breast tumors and metastases and are thought to induce genome-wide retargeting of Polycomb repressive complex 2 (PRC2) to an occupancy pattern more resembling embryonic fibroblasts, leading to altered histone H3 lysine 27 methylation, gene expression, and increased cancer invasiveness and metastasis in a manner dependent on PRC2 (22). The potential of antisense transcripts to modulate the cancer epigenome *in trans* highlights a direction in elucidating the function of such transcripts and may help to understand the role of *91H*. The absence of conservation at the protein level and the evolutionary conservation of structure at the RNA level has led to the proposal that the functional product of the *H19* gene is a structured RNA or a miRNA (23, 24).

Results and Discussion

The human genome is thought to contain far more transcripts than were previously appreciated, and up to 14% of the genome may be transcribed (25). To identify previously unappreciated transcripts in the human 11p15.5 imprinted region, we designed 278 reverse transcription (RT) and PCR primers, with a mean amplicon length of 2 kb, identifying 10 previously unappreciated transcripts in human kidney and placenta spread over 200 kb including the *H19* gene locus. To characterize the *H19* antisense transcript, we performed RT-PCR with 13 additional gene-specific RT (GS-RT) primers spanning a 7.6-kb genomic region, positioned at 0.1- to 1-kb intervals and in sense orientation to

Author contributions: P.O. and A.P.F. designed research; P.O. performed research; P.O. and A.P.F. analyzed data; and P.O. and A.P.F. wrote the paper.

The authors declare no conflict of interest.

This article is a PNAS Direct Submission.

Freely available online through the PNAS open access option.

¹To whom correspondence should be addressed. E-mail: afeinberg@jhu.edu.

This article contains supporting information online at www.pnas.org/lookup/suppl/doi:10.1073/pnas.1110904108/-DCSupplemental.

H19 (Fig. 1A). Following amplification of the cDNAs using 10 paired nested PCR primers in addition to performing 5' and 3' RACE, we found that the longest transcript was 6 kb, polyadenylated, contained a CpG island promoter, and extended 1 kb upstream and 2.8 kb downstream of *H19* (Fig. 1A–C and *SI Appendix*, Fig. S1). To confirm specificity of *HOTS* transcription, we included two negative controls, GS-RT primers without RT enzyme, and GS-RT primers with RT enzyme. The two negative control reactions failed to yield any RT-PCR amplification products (Fig. 1B). Strand-specific RT-PCR analyses of the 6-kb genomic locus failed to reveal any evidence of splicing, including the use of strand-specific RT-PCR primers initiated within the *H19* intron (RT primer: 1119R; PCR primers: 10R and 689R) or the *H19* exon (RT primer: 1R; PCR primers: 1144R and 115R) (Fig. 1A). Recently, a *H19* antisense transcript named 91H RNA with the potential to produce a 120-kb transcript was reported for the human and the mouse *H19/IGF2* loci (21). We cannot exclude the possibility that the *H19* antisense transcript that we report here could be part of 91H RNA owing to the technical limitations in both synthesis and Northern blotting of high-mo-

lecular-weight RNA. We named this smaller transcript *H19* opposite tumor suppressor (*HOTS*). Earlier studies have shown that the human *H19* locus can suppress tumor cell growth (19). We therefore focused our studies on the protein-coding potential of the ORFs contained in the *H19* antisense segment and found entirely within the *H19* transcriptional unit. The longest ORF that met this selection criteria within *HOTS* encodes a predicted polypeptide of 150 amino acids (Fig. 1D), and the +4 (purine) and –3 (purine) bases fit the Kozak consensus sequence for translation initiation (Fig. 1D). Protein database searches did not reveal any homology or functional motifs; however, we identified nuclear localization signals at residues 131 (KKKK) and 132 (K-KKR) and nuclear localization bipartite signals at 116 (KKKDR-KAOKORDRRMKK) and at 117 and 120 in *HOTS* by using the PSORT II program (<http://psort.hgc.jp/form2.html>) software (Fig. 1D).

Multiple sequence alignment revealed that *HOTS* was conserved in primates with 96% nucleotide identity in the ORF (Fig. 1E). *HOTS* was not well conserved in mouse, showing 43% identity and no ORF (*SI Appendix*, Fig. S2). *HOTS* was expressed

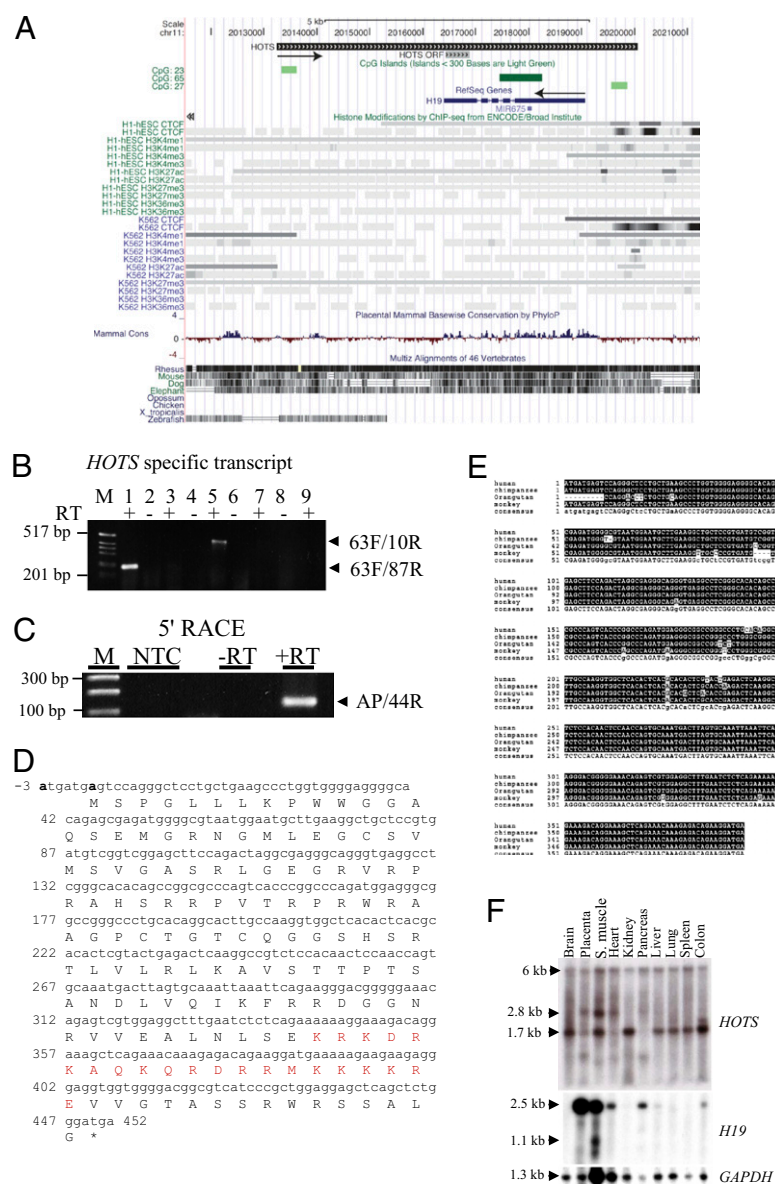


Fig. 1. *HOTS* is a primate-conserved, ubiquitous transcript antisense to *H19*. (A) Genomic organization of *HOTS* and *H19* genes on human chromosome 11p15.5. The direction of *HOTS* and *H19* transcriptional orientation is shown by black arrows. *HOTS* ORF is shown. The display is populated with CpG island (green) CTCF-binding sites, ENCODE histone modification marks, and mammalian DNA sequence conservation for the region [University of California at Santa Cruz (UCSC) on Human Genome Sequence: Feb. 2009 (GRCh37/hg19) Assembly, <http://genome.ucsc.edu/>]. (B) RT-PCR amplification of *HOTS* using strand-specific RT primer 1119R located within the first intron of *H19*, followed by amplification with intronic PCR primer pairs 63F/87R (lanes 1 and 2) and 63F/10R (lanes 5 and 6). RT-PCR amplification of *H19* using strand-specific RT primer 1F, followed by intronic PCR primer pair 63F/87R (lanes 3 and 4) or 63F/10R (lanes 7 and 8). (Lane 9) No RT primer included but RT enzyme and 63F/87R primer pair. (C) 5' RACE using primer 4534R for RT and primers 44R and PCR anchor primer. M, 1-kb DNA ladder; NTC, no template control. (D) Sequence for the *HOTS* ORF, nuclear localization signal shown in red type and the putative Kozak consensus sequences at –3 (A) and +4 (A) in boldface type. (E) Multiple sequence alignment of predicted *HOTS* primates sequences from human, chimpanzee, orangutan, and monkey. Sequence areas depicted against a black background represent identity, and small letters in the consensus sequence at the bottom show areas of sequence variability. (F) *HOTS* and *H19* human multiple tissues Northern blots. (Top) *HOTS*. (Middle) *H19*. (Bottom) *GAPDH*.

ubiquitously in all tissues tested, as shown by RT-PCR and by Northern blot hybridization with a *HOTS* strand-specific antisense RNA probe (Fig. 1*F* and *SI Appendix*, Fig. S3). The *HOTS* Northern blot shows a 6-, 2.8-, and 1.7-kb transcript, suggesting tissue-specific alternative splicing (Fig. 1*F*). *H19* was expressed only in placenta, skeletal muscle, heart, pancreas, liver, and colon (Fig. 1*F*), suggesting that the regulation of *HOTS* and *H19* might not be coordinated.

Because *H19* is uniformly described as a noncoding RNA, we took three approaches to confirm or disprove the existence of a HOTS protein. First, we assayed for association of the *HOTS* transcript with polysomes, the ribosomal protein complexes that recruit mRNAs for protein translation, an indicator that a transcript is translated. To this end, we purified RNA-associated polysomes by sucrose gradient differential centrifugation (*Methods*) from the cervical carcinoma cell lines HeLa and SiHa, human embryonic kidney 293 (HEK293) cells, and the rhabdomyosarcoma cell line RD (Fig. 2*A* and *SI Appendix*, Fig. S4). Strand-specific quantitative real-time PCR revealed preferential association of the *HOTS* transcript with polysomes, suggesting that it is translated, whereas *H19* was associated with free RNA, consistent with its being untranslated (Fig. 2*B* and *C* and *SI Appendix*, Fig. S5). As a positive control, β -actin also was preferentially associated with polysomes (Fig. 2*D*). Second, we raised a polyclonal antibody against His₆-tagged HOTS protein. We

were able to detect His-tagged HOTS with HOTS antibody and anti-His₆ antibody, as a 25-kDa protein, the additional weight beyond the expected 17 kDa is due to 9 kDa of His₆ plus trailing vector amino acid sequences, whereas no signal was obtained with preimmune serum (Fig. 2*E*). Because purified His-tagged HOTS displayed an additional signal that was twice the size of the HOTS protein's molecular weight (Fig. 2*E*), we performed immunoprecipitation to confirm if the higher band was indeed a dimer. Only the monomer band of His-tagged HOTS was detected with HOTS antibody after immunoprecipitation with anti-His₆ antibodies from HEK293 transfected cells, thus confirming the prediction that HOTS exists as a dimer in vivo (Fig. 2*E*). To determine the specificity of the HOTS antibody, we performed a Western blot on protein samples from human kidney as a positive control and on protein extracts from mouse kidney, Wilms tumor, and a BWS UPD as negative controls (Fig. 2*F*). As expected, we saw a strong positive signal only on the human kidney (Fig. 2*F*), which was specific, because it was eliminated by precompetition with purified HOTS protein (Fig. 2*F*), and there was no detectable signal in the mouse kidney (Fig. 2*F*), consistent with the sequencing data. We additionally detected on a denaturing gel a 17-kDa polypeptide using purified HOTS antibody (Fig. 2*G*). Western blot using the anti-HOTS antibody of a non-denaturing gel containing fetal tissues revealed the expected 17 kDa HOTS monomer, 34 kDa HOTS dimer, and

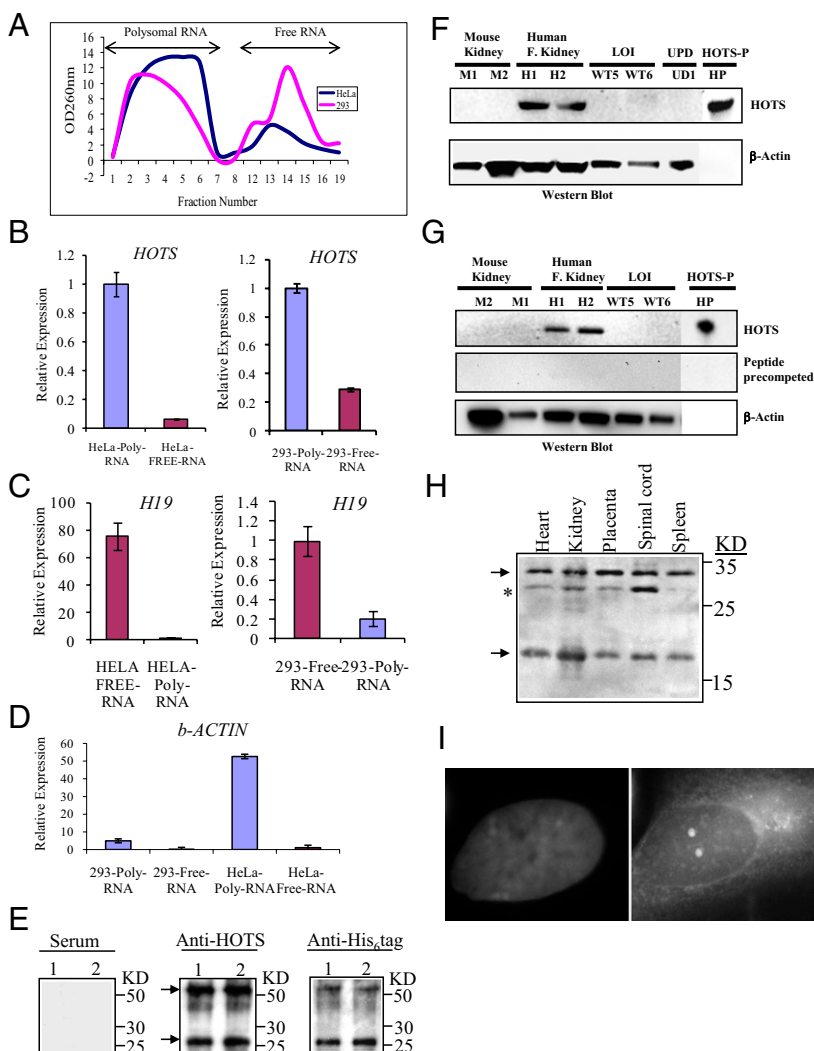


Fig. 2. *HOTS* is a polysome-associated RNA encoding a nucleolar protein. (A) Polysomal and free total cellular RNA fractionated by sucrose gradient centrifugation from homogenates of HeLa (blue) and HEK293 (pink) human cells. (B) Strand-specific quantitative real-time PCR amplification of *HOTS* transcripts shows enrichment in polysomes from HeLa and HEK293 cells, in contrast to (C) *H19*, which shows enrichment in the free RNA fraction, with (D) β -actin a positive control for polysome enrichment. (B–D) Analyses were performed in triplicate ($n = 6$). (E) Western blots of purified His₆-tag HOTS protein loaded in duplicate lanes using preimmune serum (Left), HOTS antibody (Center), and His₆-tag antibody (Right). Both the HOTS and His₆-tag antibodies detect the expected recombinant protein (arrows) of 26 kDa (17 kDa of predicted HOTS polypeptide sequence and 9 kDa of His₆ plus trailing vector amino acid sequences) and a dimer of 52 kDa. (F) Western blot with anti-HOTS antibody on protein extracts from mouse kidney (M1 and M2), human fetal kidney (H1 and H2), WTs with LOI (WT5 and WT6), a BWS sample with chromosome 11p UPD (UD1), and purified HOTS protein (HP). The LOI and UD samples are negative controls with loss of expression of the maternally expressed *HOTS*. β -Actin antibody was used on the same blot as a loading control. (G) Western blot similar to the previous but precompeted with HOTS purified protein (1 μ g/mL). (H) Western blots of a non-denaturing gel using anti-HOTS antibody on human fetal tissues. Arrows indicate the HOTS monomer of 17 kDa and a dimer of 34 kDa; asterisk indicates a 29-kDa band that might represent an isoform or posttranslationally modified protein abundant in the spinal cord. (I) Subcellular localization of native HOTS protein to the nucleolus using anti-HOTS antibody on human SiHa cells. (Left) DAPI stained nucleus. (Right) HOTS antibody image superimposed on the DAPI stain.

a differentially expressed 29 kDa isoform (Fig. 2H). Third, we investigated the subcellular localization of HOTS by transfecting Cos7 and SiHa cell lines with HOTS cDNA tagged with green fluorescence protein (GFP) in a pEGFP-N3 vector (Clontech). HOTS localized to the nucleus and was sequestered in a sub-nuclear organelle (SI Appendix, Fig. S6), confirming our earlier prediction that HOTS was a nuclear protein. Colocalization of HOTS with the nucleolar protein nucleophosmin (B23) showed that HOTS protein predominantly colocalized with nucleophosmin (SI Appendix, Fig. S7). In addition, immunohistochemical studies with the HOTS antibodies revealed nuclear and nucleolar localization (Fig. 2I).

To further validate the protein-coding potential of HOTS and to begin to understand the cellular and molecular pathways important in HOTS function, we searched for HOTS interacting proteins. Immunoprecipitation of myc-tagged HOTS from HEK293 cells revealed eight potential HOTS interacting proteins (SI Appendix, Fig. S8 and Table S1), which were then gel-purified and identified by mass spectrometry (Proteomic Research Systems). To corroborate the interaction of HOTS with each of the candidate interacting proteins, we performed immunoprecipitations from HEK293 cells cotransfected with HOTS-myc and with each potentially interacting protein tagged with His₆-V5. We confirmed by Western blot the interaction of HOTS with all eight proteins by using anti-myc antibody directed against HOTS-myc to immunoprecipitate each of the proteins detected by anti-V5 antibody. However, only one of these, human enhancer of rudimentary homolog (ERH), also showed interaction

with HOTS when we performed the reciprocal pulldown using Ni-beads to bind His₆-tagged ERH, and we detected HOTS-myc by Western blot (Fig. 3A). We could not immunoprecipitate HOTS directly with anti-HOTS antibody from HEK293 cells transfected with ERH, perhaps due to low expression levels of native HOTS. However, we immunoprecipitated HOTS-GFP using ERH antibodies (Abcam) from HEK293 cells transfected with HOTS-GFP, demonstrating that native ERH interacts with HOTS protein (Fig. 3B).

Several imprinted gene loci transcribe both an imprinted sense and an antisense transcript, including *IGF2R* and its antisense *Air* (26); *Xist* and its antisense *Tsix* (27); and *Kvlt1* and its antisense *LITI* (28). We therefore suspected that *HOTS* might also be imprinted, which we tested by exploiting a polymorphism at nucleotide +588 in the 3' UTR. Synthesis of *HOTS* cDNA using RT primers specific for HOTS transcript from the kidneys of five individuals revealed exclusive expression from only one of the two alleles found in the genomic DNA (Fig. 3C and D, and SI Appendix, Fig. S9). Genomic and fetal cDNA sequence from two informative paired maternal and fetal samples revealed the expressed allele to be of maternal origin (Fig. 3C and D).

WTs and rhabdomyosarcoma showed preferential loss of a specific parental allele in LOH, suggesting the existence of an imprinted tumor suppressor gene on 11p15 (16). Because alleles that carry an imprint are presumed to be inactive on one allele as a result of the imprinting process, tumorigenesis arising from isodisomy of the imprinted allele would have no requirement that such an allele be further mutated. Likewise, LOH affecting the normally active 11p15.5 maternal allele would be sufficient to exhibit a null (tumorigenic) phenotype. These predictions fit Sapienza's modified Knudson's "two hit" model for tumorigenesis, which incorporates genomic imprinting (16). Consistent with this model, real-time quantitative RT-PCR analysis of *HOTS* in seven WTs with LOH showed loss of expression in all cases (Fig. 4A). Furthermore, LOI of *IGF2*, which silences the maternal *H19* allele as well as activates the maternal *IGF2* allele, was also associated with *HOTS* silencing in all 10 cases tested (Fig. 4A). To rule out RNA degradation in the LOH and LOI WT samples, DNase I-treated RNA samples were separated on an agarose gel before cDNA synthesis. All but one showed a high 28S/18S ratio, and all of the samples showed abundant expression of *GAPDH* (SI Appendix, Fig. S10 and Fig. S11).

These data suggest that *HOTS* is a tumor suppressor gene. However, we did not identify mutations within the coding sequence of 30 WTs, even though mutations might not be expected for an imprinted tumor suppressor gene and are not found, for example, in the imprinted tumor suppressor gene *ARHI* in breast cancer (29). Nevertheless, to confirm the tumor suppressor activity of *HOTS*, we expressed a HOTS-GFP fusion construct and a *H19* cDNA in WT (SK-NEP-1), rhabdoid tumor (G401), rhabdomyosarcoma (RD), choriocarcinoma (JEG-3), and cervical carcinoma (SiHa) cell lines. Transfection efficiency was comparable between the native HOTS-GFP (20.2%) and mutated HOTS-GFP (21.4%) transfected cells (SI Appendix, Fig. S18). We observed potent growth inhibition in cells transfected with HOTS-GFP (SI Appendix, Table S2), whereas cell lines transfected with GFP-expressing control vector, HOTS-GFP carrying truncating mutations in HOTS, and *H19* cDNA grew to confluence with no growth inhibition (SI Appendix, Tables S2 and S3; Fig. S12).

We also considered the possibility that an overexpressed gene might show nonspecific growth inhibition or influence the expression of the counterpart sense or antisense transcript. To exclude this possibility, we performed the reverse experiment, where we knocked down *HOTS* instead of overexpressing *HOTS* and looked at reduced *HOTS* expression influence on tumor growth. We therefore generated three HeLa tumor cell lines containing tetracycline-inducible RNAi constructs for *HOTS* using the shRNA system and also directly transfected anti-HOTS siRNA

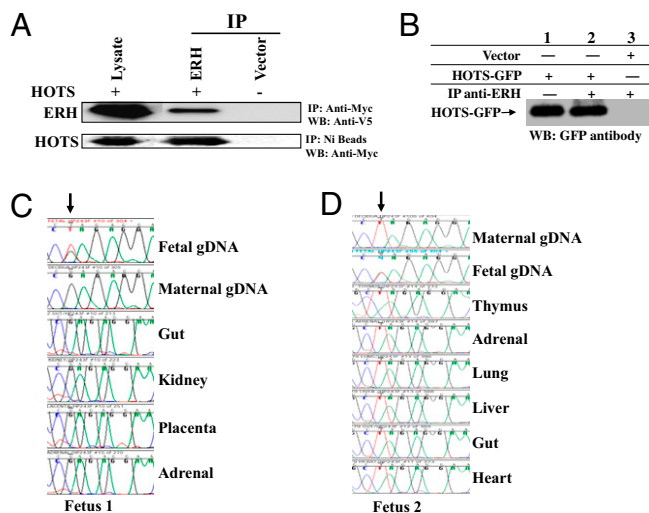


Fig. 3. HOTS interacts with ERH in vivo and is imprinted. (A) (Upper) Immunoprecipitation (IP) with anti-myc-tag antibodies specific to myc-tagged HOTS from HEK293 cells cotransfected with myc-tagged HOTS and His₆/V5-tagged ERH. V5 antibody was used to detect ERH on the Western blot (WB). (Lower) IP with nickel beads specific for His-tagged ERH from HEK293 cells transfected with myc-tagged HOTS and His₆/V5-tagged ERH; myc-tagged antibody was used to detect HOTS by WB. (B) Immunoprecipitation of HOTS from protein extracts of HEK293 cells transfected with HOTS tagged with GFP and immunoprecipitated using ERH antibody. Ten percent (30 µg) of HEK293 input extract was loaded in lane 1. Anti-GFP antibody was used for Western blot. (C) Strand-specific cDNA synthesis was carried out to study *HOTS* expression in the mother and in fetal tissues of fetus 1. The polymorphism is shown by an arrow. The maternal decidua and fetal genomic DNA sequence is included to distinguish the origin of the expressed allele. Note the exclusive expression of the maternal G allele in all fetal tissues. (D) Maternal T allele expression in all fetus 2 tissues (indicated by an arrow). Note that the fetus genomic DNA is heterozygous and therefore informative for allele-specific gene expression. All cDNA synthesis was performed with gene-specific primers that produced only *HOTS* transcripts.

targeted to the nucleus and sequestered in the nucleolus. WT_s with LOI of *H19* or LOH of human chromosomal band 11p15.5 lose *HOTS* expression. Expression of *HOTS* in cancer cell lines inhibits tumor cell growth, and silencing of *HOTS* promotes in vitro anchorage-independent growth and in vivo tumorigenicity. Because *HOTS* is imprinted and its expression is lost in WT_s with both LOH and LOI, it fits the predictions for an imprinted tumor suppressor gene (16). As such, it is at least one member of the WT2 gene locus on 11p15.

We also identified at least one protein that interacts with *HOTS*, namely ERH. ERH has been shown to be important in pyrimidine biosynthesis, cell cycle regulation, and transcriptional repression (30). ERH is known to interact with the zinc-finger protein CIZ1, a promoter of DNA replication that interacts with p21 (Cip1), a CDK2 inhibitor critical for cell cycle regulation (31). Moreover, ERH interacts with SKAR, a cell growth regulator in the S6K1-signaling pathway (32). We propose from these protein interactions that *HOTS* may mediate its tumor suppressor activity by targeting DNA replication and cell cycle regulation.

Finally, we note that *HOTS* joins a relatively small group of primate-specific proteins, including the *POTE* (expressed in prostate, ovary, testis, and placenta) gene family (33) and MGC8902, a human lineage-specific protein thought to be involved in higher cortical function (34).

Methods

HOTS cloning was performed by RT-PCR, and a full-length ORF was cloned into pEGFP.N3 and p3XFLAG-Myc-CMV-24 plasmid vectors. To generate riboprobes, partial *HOTS/H19* sequences were cloned into the pCRII TOPO T7/Sp6 vector. Polysome association of *HOTS* transcript was investigated by purification of free and polysome-associated RNA by using sucrose gradient differential centrifugation, and transcript levels were measured by quantitative real time PCR using internal controls. To generate *HOTS* antibody, we cloned *HOTS* into the bacterial expression vector pDEST17 and purified His₆-tagged proteins. For subcellular localization, we used *HOTS* antibodies and also transfected Cos-7 cells with *HOTS* cloned in pEGFP.N3 by lipofection and stained organelles using specific antibodies. Tumor growth assays were performed with wild-type and mutated *HOTS* cloned in pEGFP.N3 and transfected into SiHa, Cos7, RD, JEG-3, SK-NEP-1, and G401 cells. To study *HOTS* knockdown on tumor cell growth, we cloned shRNA targeting *HOTS* into the tetracycline-inducible pENTR H1/TO vector and transfected HeLa-TREx cells by lipofection, generating stable cell lines. Tumor growth effects were studied by both soft agar assay and in vivo in athymic nude mice. To identify *HOTS*-interacting proteins, we transfected HEK293 cells with *HOTS* in p3XFLAG-Myc-CMV-24 and used anti-cmyc antibodies to immunoprecipitate interacting proteins that were subjected to mass spectrometry for identification. Candidate *HOTS*-interacting proteins were isolated by RT-PCR and cloned into the pEF6/V5-His TOPO TA vector and were validated by coimmunoprecipitation and Western blot analysis. See *SI Appendix* for full description of methods.

ACKNOWLEDGMENTS. This work was supported by National Institutes of Health Grant CA65435 (to A.P.F.).

- Arney KL (2003) H19 and Igf2: Enhancing the confusion? *Trends Genet* 19:17–23.
- Tremblay KD, Duran KL, Bartolomei MS (1997) A 5' 2-kilobase-pair region of the imprinted mouse H19 gene exhibits exclusive paternal methylation throughout development. *Mol Cell Biol* 17:4322–4329.
- Thorvaldsen JL, Duran KL, Bartolomei MS (1998) Deletion of the H19 differentially methylated domain results in loss of imprinted expression of H19 and Igf2. *Genes Dev* 12:3693–3702.
- Ripoche MA, Kress C, Poirier F, Dandolo L (1997) Deletion of the H19 transcription unit reveals the existence of a putative imprinting control element. *Genes Dev* 11:1596–1604.
- Hark AT, et al. (2000) CTCF mediates methylation-sensitive enhancer-blocking activity at the H19/Igf2 locus. *Nature* 405:486–489.
- Bell AC, Felsenfeld G (2000) Methylation of a CTCF-dependent boundary controls imprinted expression of the Igf2 gene. *Nature* 405:482–485.
- Jones BK, Levorse JM, Tilghman SM (1998) Igf2 imprinting does not require its own DNA methylation or H19 RNA. *Genes Dev* 12:2200–2207.
- Leighton PA, Ingram RS, Eggenschwiler J, Efstratiadis A, Tilghman SM (1995) Disruption of imprinting caused by deletion of the H19 gene region in mice. *Nature* 375:34–39.
- Rainier S, et al. (1993) Relaxation of imprinted genes in human cancer. *Nature* 362:747–749.
- Weksberg R, et al. (2001) Tumor development in the Beckwith-Wiedemann syndrome is associated with a variety of constitutional molecular 11p15 alterations including imprinting defects of KCNQ1OT1. *Hum Mol Genet* 10:2989–3000.
- Feinberg AP, Tycko B (2004) The history of cancer epigenetics. *Nat Rev Cancer* 4:143–153.
- Sparago A, et al. (2004) Microdeletions in the human H19 DMR result in loss of IGF2 imprinting and Beckwith-Wiedemann syndrome. *Nat Genet* 36:958–960.
- Feinberg AP, Williams BR (2003) Wilms tumor as a model for cancer biology. *Tumor Suppressor Genes*, ed El-Deiry WS (Humana, Totowa, NJ), Vol 1, pp 239–248.
- Dao D, et al. (1999) Multipoint analysis of human chromosome 11p15/mouse distal chromosome 7: Inclusion of H19/Igf2 in the minimal WT2 region, gene specificity of H19 silencing in Wilms' tumorigenesis and methylation hyper-dependence of H19 imprinting. *Hum Mol Genet* 8:1337–1352.
- Karnik P, Chen P, Paris M, Yeger H, Williams BR (1998) Loss of heterozygosity at chromosome 11p15 in Wilms tumors: Identification of two independent regions. *Oncogene* 17:237–240.
- Scrabble H, et al. (1989) A model for embryonal rhabdomyosarcoma tumorigenesis that involves genome imprinting. *Proc Natl Acad Sci USA* 86:7480–7484.
- Overall ML, Spencer J, Bakker M, Dziadek M, Smith PJ (1996) p57K1P2 is expressed in Wilms' tumor with LOH of 11p15.5. *Genes Chromosomes Cancer* 17:56–59.
- Rachmilewitz J, et al. (1995) H19 expression and tumorigenicity of choriocarcinoma derived cell lines. *Oncogene* 11:863–870.
- Hao Y, Crenshaw T, Moulton T, Newcomb E, Tycko B (1993) Tumour-suppressor activity of H19 RNA. *Nature* 365:764–767.
- Tsang WP, et al. (2010) Oncofetal H19-derived miR-675 regulates tumor suppressor RB in human colorectal cancer. *Carcinogenesis* 31:350–358.
- Berteaux N, et al. (2008) A novel H19 antisense RNA overexpressed in breast cancer contributes to paternal IGF2 expression. *Mol Cell Biol* 28:6731–6745.
- Gupta RA, et al. (2010) Long non-coding RNA HOTAIR reprograms chromatin state to promote cancer metastasis. *Nature* 464:1071–1076.
- Juan V, Crain C, Wilson C (2000) Evidence for evolutionarily conserved secondary structure in the H19 tumor suppressor RNA. *Nucleic Acids Res* 28:1221–1227.
- Cai X, Cullen BR (2007) The imprinted H19 noncoding RNA is a primary microRNA precursor. *RNA* 13:313–316.
- ENCODE Project Consortium; Birney E, et al. (2007) Identification and analysis of functional elements in 1% of the human genome by the ENCODE pilot project. *Nature* 447:799–816.
- Lyle R, et al. (2000) The imprinted antisense RNA at the Igf2r locus overlaps but does not imprint Mas1. *Nat Genet* 25:19–21.
- Lee JT, Davidow LS, Warshawsky D (1999) Tsix, a gene antisense to Xist at the X-inactivation centre. *Nat Genet* 21:400–404.
- Lee MP, et al. (1999) Loss of imprinting of a paternally expressed transcript, with antisense orientation to KVLQT1, occurs frequently in Beckwith-Wiedemann syndrome and is independent of insulin-like growth factor II imprinting. *Proc Natl Acad Sci USA* 96:5203–5208.
- Yu Y, et al. (1999) NOEY2 (ARHI), an imprinted putative tumor suppressor gene in ovarian and breast carcinomas. *Proc Natl Acad Sci USA* 96:214–219.
- Jin T, Guo F, Serebriiskii IG, Howard A, Zhang YZ (2007) A 1.55 Å resolution X-ray crystal structure of HEF2/ERH and insights into its transcriptional and cell-cycle interaction networks. *Proteins* 68:427–437.
- Coverley D, Marr J, Ainscough J (2005) Ciz1 promotes mammalian DNA replication. *J Cell Sci* 118:101–112.
- Richardson CJ, et al. (2004) SKAR is a specific target of S6 kinase 1 in cell growth control. *Curr Biol* 14:1540–1549.
- Bera TK, et al. (2002) POTE, a highly homologous gene family located on numerous chromosomes and expressed in prostate, ovary, testis, placenta, and prostate cancer. *Proc Natl Acad Sci USA* 99:16975–16980.
- Popesco MC, et al. (2006) Human lineage-specific amplification, selection, and neuronal expression of DUF1220 domains. *Science* 313:1304–1307.